Black carbon radiative forcing derived from AERONET measurements and models over an urban location in the southeastern Iberian Peninsula

Valenzuela, A.[1, 2,3], Arola, A.[4] Antón, M.[5], Quirantes, A.[2] Alados-Arboledas, L.[2, 3]

[1] *Departamento de Física, Instituto de Ciências da Terra, Instituto de Investigação e Formação Avançada, Universidade de Évora, Évora (Portugal)*

[2]*Departamento de Física Aplicada, Universidad de Granada, Granada, Spain*

[3]*Andalusian Institute for Earth System Research (IISTA-CEAMA), Granada, Spain*

[4]*Finnish Meteorological Institute (FMI), Kuopio, Finland*

[5]*Departamento de Física, Universidad de Extremadura, Badajoz, Spain*

Keywords: aerosol particles, anthropogenic aerosol, black carbon, shortwave radiative forcing.

Abstract

This paper provides an account of observed variations in Black carbon (BC) aerosol concentrations and their induced radiative forcing for the first time over Granada a measurement site in Southeastern Iberian Peninsula. Column-integrated BC concentrations were retrieved for the period 2005-2012. Monthly averages of BC concentrations (± one standard deviation) ranged from higher values in January and December with 4.0±2.5 and 4±3 mg/m^2, respectively, to lower values in July and August with 1.6±1.2 and

2.0±0.5mg/m^2, respectively. This reduction is not only observed in the average values, but also in the median, third and first quartiles. The average BC concentration in winter (3.8±0.6 mg/m^2) was substantially higher than in summer (1.9±0.3 mg/m^2), being the eight-year average of 2.9±0.9 mg/m^2. The reduction in the use of fossil fuels during the economic crisis contributed significantly to reduced atmospheric loadings of BC. According to our analysis this situation persisted until 2010. BC concentration values were analyzed in terms of air mass influence using cluster analysis. BC concentrations for cluster 1 (local and regional areas) showed high correlations with air masses frequency in winter and autumn. In these seasons BC sources were related to the intense road traffic and increased BC emissions from domestic heating. High BC concentrations were found in autumn just when air mass frequencies for cluster 3 (Mediterranean region) were more elevated, suggesting that air masses coming from that area transport biomass burning particles towards Granada. BC aerosol optical properties were retrieved from BC fraction using aerosol AERONET size volume distribution and Mie theory. A radiative transfer model (SBDART) was used to estimate the aerosol radiative forcing separately for composite aerosol (total aerosols) and exclusively for BC aerosols. The mean radiative forcing for composite aerosol was +23±6 W/m^2 (heating rate of +0.21±0.06 K/day) and +15±6 W/m^2 for BC aerosol (heating rate of +0.15±0.06 K/day). These values of radiative forcing and heating rate for BC aerosol represent about 70% of their values for composite aerosol, which highlights the crucial role that BC aerosols play in modifying the radiation budget and climate.

1. Introduction

Black carbon (BC) is the dominant absorbing aerosol in the solar radiation spectrum, playing a key role in the estimation of the direct radiative forcing although it accounts for less than 5% of the mass of atmospheric aerosol in most areas of the world (Haywood and Since, 1997; Zhang et al., 2012). Bond et al. (2013) provided an inventory of the major BC sources. They are listed according to the importance of emission: The bottom-up estimates predicts that open burning contributes about 40% of total BC emissions. Residential Solid Fuels (Wood, agricultural waste, dung, and coal) provide another 25% of BC emissions. The diesel-engine category (on-road and off-road engines) is estimated that contributed about 20% of global BC emissions of the total. Finally, industrial coal combustion is estimated to provide about 9% of global emissions. BC is directly emitted into the air from these sources, not formed in the atmosphere from precursor substances. Estimates of BC global annual emissions were 8.0 Tg. The uncertainties were about a factor of 2, with uncertainty range of 4.3–22 Tg/yr. BC particles are generally produced from the incomplete combustion of fossil fuels and biomass burning (Zhao et al., 2015). BC can raise the amount of solar radiation absorbed in the visible and infrared spectral ranges within the Earth's climate system and, consequently, heat the atmosphere and surface (Hansen et al., 2000; Ramanathan and Carmichael, 2008). Ramanathan and Carmichael (2008) performed a comparison of radiative forcing caused by greenhouse gases and BC. They found that the direct radiative forcing due to BC was larger than that due to any other greenhouse gas except CO_2. BC causes large atmospheric warming constituting about 55% of CO_2 forcing on the global scale (Ramanathan and Carmichael, 2008; Keil et al., 2001; Babu et al., 2002; Bond et al., 2013). Bond et al. (2013) estimated a climate forcing due to BC of +1.1W/m^2

with 90% uncertainty limits of +0.17 to +2.1W/m^2. The process through which BC suspended in the atmosphere scatters and absorbs incoming solar radiation is termed ‘’ direct effect’’. The absorption by BC suspended warms the air, but the extinction of radiation results a negative forcing at the Earth’s surface (Ramanathan and Carmichael, 2008). The ‘’semi-direct effect’’ assumes that BC particles reside interstitially between cloud droplets (Johnson, 2004; Chung and Seinfeld, 2005; Jacobson, 2006; Jones et al., 2007). BC also has significant effects on clouds by changing atmospheric stability, affecting cloud formation (Ackerman et al., 2000). Therefore, BC is considered as a potential cause of global warming (Hansen et al., 2000; Bond et al., 2013). BC may also play a relevant role for the aerosol cloud (“indirect effect”) since it is injected into the atmosphere as primary aerosol particle, affecting the number of particles available in cloud condensation (Oshima et al., 2009).

There are a large number of papers focused on the analysis of aerosol measurements over the Iberian Peninsula (e.g., Silva et al., 2002; Olmo et al., 2006; Estellés et al., 2007; Cachorro et al., 2008; Prats et al., 2008; Toledano et al., 2009; Pereira et al., 2011; Valenzuela 2012a). However, none of them were focused on studying the BC aerosol in this region. To our knowledge, only Lyamani et al. (2011) performed a detailed analysis about BC concentration at the surface level. They measured significant amount of BC over surface in Granada with mean value of 3.0±1.5 µg/m^3. These authors also reported that BC exhibited a well-defined seasonal variation with the highest concentration during winter likely due to increased emissions from domestic heating and a lower planetary layer height (Granados et al., 2012). The disadvantage of in situ measurements is that require considerable effort and this technique does not provide large spatial and temporal coverage

(Derimian et al., 2008). Recently, some studies have paid attention to retrieve aerosol composition from AERONET retrievals, since it provides worthy information on aerosol optical and physical properties such as column-averaged aerosol refractive indices and size distributions (Schuster et al., 2005; Dey et al., 2006; Arola et al., 2011). They derived information of BC concentration from AERONET imaginary refractive indices assumes that absorption is due to three components: Black Carbon (BC), Brown Carbon (BrC) and mineral dust (MD). In addition, it can also provide a long term view and extensive spatial coverage, as it comprises more than 300 sun photometers placed throughout the world (Holben et al., 1998).

Long-range transport of BC has a great significance on the climate change and air quality. However, large uncertainties remain between simulated and observed global transport of BC. Uncertainties in models result from many factors, including BC emissions inventories, the parameterizations of BC aging, wet removal, and dry deposition processes (Liu et al., 2011; Shen et al., 2014). BC aging process occurring during long-range transport is a key factor in simulated concentrations of BC. The aging process refers to a transformation from hydrophobic to hydrophilic aerosols, where aged BC particles can act as CCN and, thus, they can be removed by wet scavenging when BC is trapped in cloud droplets or ice crystals. From all pathways for the hydrophobic-to-hydrophilic conversion, chemical aging is the least understood, but potentially could affect hydrophobic-to-hydrophilic conversion on time scales shorter than days or weeks (Kanakidou et al., 2005). Therefore, the rate of aging significantly affects the atmospheric lifetime of BC, being one of the key factors controlling long-range transport of these particles and, consequently, affecting their global

distribution (Liu et al., 2011). However, the aging of BC is highly simplified in global models and, thus, errors related to the BC wet scavenging should be taken into account.

Backward trajectory analysis is a well-known technique to link air mass-origin with aerosol optical properties at the measurements area (e.g. Kokkalis et al., 2017; Kumar et al., 2017; Zdun et al., 2016; Valenzuela et al., 2015). The analysis of backward trajectories provides objective interpretations related to source regions, residence times over each region and different circulation patterns (curvature and length) of air masses. The accuracy of back-trajectories showed position errors with the travel's distance (Stohl, 1998). These errors produce divergence in the back-trajectories and they are associated with five causes (Harris et al., 2005): differences in computational methodology, 3–4%; time interpolation, 9–25%; vertical movement method, 18–34%; meteorological input data, 30–40%; and combined two-way differences in vertical transport method and meteorological input data, 39–47%. This sensitivity test was performed for 96 hours of flight time. In other studies, seven-day back trajectory calculations were done taking into account the aerosols residence time of around one week in the lower atmosphere in the northern midlatitudes (Kumar Bharath, d. and S. Verma, 2016).

Some studies have focused on the characterization of the aerosol radiative forcing during desert dust events over southeastern Iberian Peninsula (e.g., Anton, et al., 2012; Valenzuela et al., 2012b). However, to our knowledge, no study has addressed the characterization of the BC content in the entire atmospheric column and their radiative effects over the southeastern Iberian Peninsula. Hence, it is a challenge to carry out the first study of BC content retrieved from sun-photometer measurements over southeastern Iberian Peninsula,

especially considering that is has relevance not only from the local point of view, but also from a regional perspective. Thus we develop a detailed analysis of BC aerosol in Granada urban atmosphere for the period 2005-2012. Furthermore, the BC radiative effects in the shortwave spectral range will be determined and, compared with the radiative effects of the total aerosol (composite aerosol), although restricted to fine mode-dominated cases.

1. Experimental site, instrumentation and data

Ground-based data were retrieved at the radiometric station located on the rooftop of the Andalusian Institute for Earth System Research (IISTA-CEAMA, 37.168N, 3.608W) in Granada (South-Eastern Spain) which is found at 680 m a.s.l. (Figure 1). Granada is a medium-sized city with little emissions associated with large-scale industrial activities and with a population of 300,000 inhabitants. However anthropogenic fine aerosols load are expected from domestic heating and intense road traffic in the city and metropolitan area (Lyamani et al., 2011). The city is found in a natural basin close to Sierra Nevada's mountain range to the southeastern with elevations between 1000 and 3500 m a.s.l. The is frequently affected by air masses coming from the Atlantic Ocean, the European and African continents, and less frequently from the Mediterranean Sea (Lyamani et al., 2010).

Total columnar aerosol properties were retrieved from measurements of CIMEL CE-318 sun-photometer which is included in the AERONET network (Holben et al., 1998). This instrument makes direct sun measurements with a 1.2° full field of view at 340, 380, 440, 500, 675, 870 and 1020 nm. The full-width at half-maximum of the interference filters are 2 nm at 340 nm, 4 nm at 380 nm and 10 nm at all other wavelengths. The sky radiance measurements (almucantar configuration) are carried out at 440, 675, 870 and 1020 nm.

The characteristics of the CIMEL sun-photometer are fully described by Holben et al. (1998). The direct sun measurements are used to compute the aerosol optical depth (AOD) at 340, 380, 440, 670, 870 and 1020 nm (Holben et al., 1998). The uncertainty in the retrieval of AOD under cloud free conditions is ±0.01 for wavelengths larger than 440 nm and ±0.02 for shorter wavelengths (Eck et al., 1999). Sky radiance measurements together with solar direct irradiance measurements are used to retrieve aerosol optical properties like single scattering albedo, $\omega(\lambda)$, using the AERONET inversion algorithm developed by Dubovik and King (2000) as improved by Dubovik et al. (2006). The uncertainty in the retrieval of $\omega(\lambda)$ is ±0.03 for high aerosol load (AOD (440 nm) > 0.4) and solar zenith angle > 50°. For measurements with low aerosol load (AOD(440 nm) < 0.2), the retrieval accuracy of $\omega(\lambda)$, drops down to 0.02-0.07 (Dubovik et al., 2000).

2. Methodology

3.1 BC content

The technique used by Arola et al. (2011) has been utilized in this work to retrieve information about BC aerosol concentration. This method is based on the approach employed previously by Schuster et al. (2005). Further information regarding the method can be found in the mentioned works. Thus, AERONET measurements of refractive index and the above mentioned approach were used to retrieve information about BC aerosol fraction. For a mixture of BC, BrC and Ammonium Sulfate $(NH_4)_2(SO_4)$ embedded in water host the Maxwell-Garnett (MG) mixing rule was applied. Similar refractive index values for all components as those suggested by Arola et al. (2011) were considered. In the present work, it is assumed that BrC was responsible for absorption at the ultraviolet

spectral range that cannot be explained by BC. Considering all the inclusions as spherical, the effective dielectric constant for the mixture (ε_{MG}) follows the equation given by (Bohren and Huffman, 1998, p.217):

$$\varepsilon_{MG} = \varepsilon_m \left[1 + \frac{3\left(f_1 \frac{\varepsilon_1 - \varepsilon_m}{\varepsilon_1 + 2\varepsilon_m} + f_2 \frac{\varepsilon_2 - \varepsilon_m}{\varepsilon_2 + 2\varepsilon_m} + f_3 \frac{\varepsilon_3 - \varepsilon_m}{\varepsilon_3 + 2\varepsilon_m} \right)}{1 - \left(f_1 \frac{\varepsilon_1 - \varepsilon_m}{\varepsilon_1 + 2\varepsilon_m} - f_2 \frac{\varepsilon_2 - \varepsilon_m}{\varepsilon_2 + 2\varepsilon_m} - f_3 \frac{\varepsilon_3 - \varepsilon_m}{\varepsilon_3 + 2\varepsilon_m} \right)} \right] \quad (1)$$

where ε_m, ε_1, ε_2 and ε_3 are the dielectric constant of the host matrix (water), BC, Ammonium Sulfate and BrC and f_1, f_2 and f_3 are the corresponding volume fractions of BC, Ammonium Sulfate and BrC, respectively.

MG provides the average dielectric constant of the mixture, from which the real n(λ) and imaginary k(λ) refractive index of mixture have been determined according to the following expressions (Bohren and Huffman, 1998):

$$k(\lambda) = \sqrt{\frac{\sqrt{\varepsilon_r^{\,2} + \varepsilon_i^{\,2}} - \varepsilon_r}{2}} \quad (2)$$

$$n(\lambda) = \sqrt{\frac{\sqrt{\varepsilon_r^{\,2} + \varepsilon_i^{\,2}} + \varepsilon_r}{2}} \quad (3)$$

where ε_r and ε_i are the real and imaginary parts of the mixture dielectric constant. According to MG, first, k(λ) has been retrieved taking into account different combinations of f_1 and f_3. The objective is to determine the appropriate volume fractions of f_1 and f_3.

They were adjusted until the χ^2 fit of the computed k(λ) of the mixture was minimized with respect to the AERONET retrieved k(λ) values by:

$$\chi^2 = \sum_{i=1}^{4} \frac{(k_i^{rtv} - k_i^{cal})^2}{(k_i^{rtv})^2} \tag{4}$$

where k_i^{rtv} is the imaginary refractive index retrieved from sun photometer measurements and k_i^{cal} is the value obtained from MG mixing rule, i being the summation index over four wavelengths (440, 675, 870 and 1020 nm) of AERONET. Once the calculated k(λ) matches to sun-photometer retrieved k(λ) within certain limit (χ^2 in the order of 10^{-3}), the volume fraction of Ammonium Sulfate (f_2) is adjusted to minimize χ^2 fit for n(λ). The volume fractions of all the components for which χ^2 values for k(λ) and for n(λ) are the lowest, are chosen as the best values to retrieve BC concentration. In our study, column-integrated BrC concentration was found to vary in a wide range 2.5–12.5 mg/m^2 for the entire period. A value for BC density (ρ_{BC}) of 1.8 g/cm^3 was assumed and the column-integrated aerosol volume size distributions from AERONET were considered to retrieve BC concentration:

$$BC = f_1 \rho_{BC} \int \frac{dV}{d\ln r} d\ln r\,, \tag{5}$$

where r is the particle radius in microns and V is the particle volume concentration (μm^3/μm^2). Dust dominated cases were excluded, and only those retrievals with ratio of fine mode to total volume concentration larger than 0.5 were taken into consideration.

3.2 Air mass transport

Source-receptor relationships between the measurement areas and the potential emission sources are investigated with the use of the particle dispersion model HYSPLIT_4 model. Five-day back-trajectories of air mass arriving to Granada at 500, 1500 and 3000 m a.g.l. were computed using HYSPLIT_4 model including vertical wind (Draxler and Hess, 1998) coincident with BC observation days. In our work, the back-trajectories were computed for 120 hours of flight time as a compromise between accuracy and the need to reconstruct as complete as possible the average life cycle of aerosol particles in the atmosphere. The NCEP/NCAR reanalysis database was used as meteorological file input (NOAA Operational Model Archive Distribution System server at NCEP). First, for each day, one single trajectory at each altitude level was computed with endpoint in Granada at 12:00 UTC. Additionally, a visual inspection of the back trajectories was performed at all levels with the goal of checking that air mass arriving to Granada never overpasses North Africa. To get information about air flow patterns, a statistical methodology was applied to a dataset of 265 back trajectories over Granada. This classification method was based on the geometric distance between individual back trajectories, taking into account the speed and direction of the back trajectories. The results are clusters-mean which grouping individual back trajectories with similar behavior. Air masses affecting Granada from 2005 to 2012, when BC concentration was available, were classified according to their transport pathways using HYSPLIT clustering algorithm (http://www.arl.noaa.gov/). The back trajectory types were considered in terms of the permanent synoptic situations. Large scale circulation features were related to certain trajectory centroids. The cluster analysis does not assume

the existence of BC sources and their geographic locations for clustering the back trajectory types. The centroid represents the average of the trajectories included in that cluster. HYSPLIT model hold a tool for clustering based on the variations in both the total variance between clusters (TSV, Spatial Variance Total) and the variance between each component of back trajectory (SPVAR, Spatial Variance) (Draxler et al., 2009). First, a set of 265 back-trajectories arriving over Granada was obtained. An initial number of back trajectories were chosen and, after grouping process, the result was a single cluster as average back trajectory of some of them. After that, two trajectories were grouped at each step which created smaller increase of TSV and SPAVR. Large changes were indicative of the conglomerating of large different trajectories into the same cluster. Accordingly, the best representation in the number of groups is just before the large percentage of change in TSV. Four groups for 500 m a.g.l. were chosen in order to a better explanation of the air mass transport regimes during the study period after additional analysis for different cluster numbers. Within each cluster, individual trajectories were averaged to produce a cluster-mean trajectory. The flow patterns of air masses at 1500 and 3000 m a.g.l. were similar to the flow patterns retrieved at 500 m a.g.l.

3.3 Calculation of radiative effects

Both, aerosol optical properties for composite aerosol and exclusively for BC aerosol were independently used as input in Santa Barbara Discrete-ordinate Atmospheric Radiative Transfer model (SBDART) (Ricchiazzi et al., 1998) to derive instantaneous net fluxes (down-up) in the 310-2800 nm spectral range at the surface and the top of the atmosphere (TOA). Radiative transfer code characterizes atmospheric aerosol radiative effects using the

solar zenith angle, the spectral aerosol optical depth (AOD), the spectral single scattering albedo (ω), and the spectral asymmetry parameter (g) as input values. Regarding the vertical distribution of aerosol, the SBDART profile was used which takes into account the aerosol-loaded atmosphere fitting an exponential-decay to the aerosol optical depth derived by sun-photometer. Total ozone column derived from the Ozone Monitoring Instrument (OMI) satellite and the surface spectral albedo provided by the AERONET algorithm, based on dynamic spectral and spatial model estimation at four wavelengths: 440, 675, 870 and 1020 nm were used as input in the model. Surface albedo is a very decisive input for calculating the aerosol radiative effect. It was linearly interpolated between the retrieved wavelength values. The surface albedo value at 440 nm was extrapolated to the shorter wavelengths as well, while the wavelengths larger than 1020 nm were linearly extrapolated.

Size distributions and BC fractions were used to calculate the aerosol optical properties for the BC, which was based on the Mie theory. Likewise, both the "composite aerosol" and the "BC aerosol" were described by their respective spectral AOD, ω and g, which were finally used to estimate the radiative effects.

The instantaneous aerosol radiative forcing for composite aerosol (ARF) at the surface (TOA) is obtained as:

$$ARF = F - F^{0} \tag{6}$$

where F and F^0 denote the shortwave net fluxes at surface (TOA) simulated with aerosol information related to composite aerosol and without aerosol information , respectively.

Following an identical procedure, the instantaneous aerosol radiative forcing for BC aerosol (BCRF) at the surface (TOA) is obtained as:

$$BCRF = F_{BC} - F^{0} \tag{7}$$

where F_{BC} is now the shortwave net flux at surface (TOA) simulated with aerosol information but related exclusively to BC aerosol.

Daily mean values of both ARF and BCRF at the surface (TOA) are derived from integration of the instantaneous forcing values at surface (TOA) averaged 24 hours (Bush and Valero, 2003; Valenzuela et al., 2012):

$$ARF_{daily} = \int \frac{ARF\ dt}{24}, \tag{8}$$

$$BCRF_{daily} = \int \frac{BCRF\ dt}{24} \tag{9}$$

Heating rate was determined according to the finite difference estimates of the irradiance divergence at each pair of levels (Liou, 2002);

$$\frac{\partial T}{\partial t} = \frac{g}{C_p} \frac{\Delta F_{Atmosferic}}{\Delta p} \tag{10}$$

where T is the temperature (K), t is the time (s), g is the gravitational acceleration (9.8 m/s^2), C_p is the specific heat (~1004 J/kgK), F is the net all-wave flux (W/m^2), and p is the pressure (Pa). The relative standard error in radiative forcing and heating rate reported here, taking into account the aerosol input parameters, uncertainties in BC concentrations, and flux estimates, is estimated to be 25%.

4. Results and discussion

4.1. Temporal variation of BC content

BC aerosol concentrations were retrieved from 734 sun-photometer observations corresponding to 265 days from 2005 to 2012 over Granada. BC concentrations exhibited clear seasonal pattern, evident in the monthly BC concentrations observed during the entire period (Fig. 2). The monthly mean BC concentrations were high in winter (December to February) and autumn (September to November) and low in summer (June to August) and spring (March to May), with the highest concentrations in winter and the lowest in summer. Vertical bars in boxes denote ±one standard deviation, which indicates the variability in the BC concentrations measured each month. The monthly-averaged BC concentrations for the entire analyzed period were 4.0±2.5 and 4 ±3 mg/m^2, for December and January, respectively, and 1.6±1.2 and 2.0±0.5 mg/m^2 for July and August, respectively, in agreement with typical values of European urban environment as reported by Shuster et al. (2005). The average BC concentration in winter was more than three times that computed in summer. The winter average BC concentration (3.8±0.6 mg/m^2) was 30% higher than the eight-year average (2.9±0.9 mg/m^2) whereas the summer average BC concentration (1.9±0.3 mg/m^2) was 35% lower than the overall mean. This seasonal variation in BC concentrations in atmospheric column is similar to the seasonal variations at ground level, derived for other aerosol properties in the study area (Lyamani et al., 2010; Lyamani et al., 2011). The seasonal mean BC concentrations for the entire analyzed period were 3.8±0.6, 2.05±0.03, 1.9±0.3 and 3.4±0.2 mg/m^2 for winter, spring, summer and autumn, respectively. In the same way that other studies (e.g., Dey et al., 2006), BC concentration

was assumed well mixed below the boundary layer height (h). Consequently, BC concentration retrieved in the atmospheric columnar can be converted to surface BC concentrations dividing by h. Typical h values in this area were 1.4±0.2, 1.7±0.3, 2.0±0.6 and 1.6±0.4 km for winter, spring, summer and autumn, respectively (Granados-Muñoz et al., 2012). Thus, corresponding seasonal mean values of surface BC concentrations values were 2.7, 1.2, 0.9 and 2.2 μg/m^3. Mean value retrieved in our study in winter was notably lower that retrieved by Lyamani et al. (2011) at surface level in this season (4.4 μg/m^3). Additionally, seasonal BC concentration variability in the atmospheric column presented a behavior similar to that found by Lyamani et al. (2011) at the surface level. Thus, BC showed an evident smooth decreasing in warm seasons and slightly increasing in cold seasons. The features of BC concentration in the atmospheric column is related to a combination of synoptic patterns and their associated wind flows with air mass coming from different source areas. Moreover, different emission rate by polluted urban sources could also produce a lesser extent in the seasonal BC variability changes. The main BC emission sources could be the diesel fuel combustion processes, such as motor vehicles, which remain throughout the year, and domestic heating emission in winter time. Similar seasonal variations in BC concentrations have been observed in other urban areas (e.g. Ramachandran and Rajesh, 2007; Kirchstetter et al., 2008; Cao et al., 2009; Saha and Despiau, 2009), with higher BC concentrations in winter. Theses authors attributed the high BC concentrations in winter to the increase in anthropogenic activities associated with domestic heating, in addition to unfavorable meteorological conditions like shallow atmospheric boundary layer and low wind speed.

The year-to-year evolution of the BC concentration from 2005 to 2012 is shown in Figure 3. The annual mean BC concentrations exhibited similar values during 2005 and 2006 (3.0±2.0 and 3.2±2.4 mg/m^2, respectively), showing a notable increase in 2007 (4.0±2.4 mg/m^2). From 2008, a strong reduction is observed, reaching low BC concentrations in 2009 (1.0±0.7 mg/m^2) and 2010 (1.4±1.1 mg/m^2). This annual BC reduction is in agreement with the results reported by Lyamani et al. (2011). These authors associated this BC concentration reduction with the effect of the economic crisis. In our study, the analysis has been extended until 2012 confirming that annual mean BC concentration reduction remained until 2010. The BC levels for 2011 and 2012 showed slight increasing with annual mean values of 2.3±1.8 and 2.5±1.8 mg/m^2, respectively. Nevertheless, these two years still showed BC values lower than those registered in the years previous to the start of the economic crisis. The annual report offered by Energy National committee (www.cne.es) indicates that the sales of combustibles derived from petrol dropped from 2007 to 2012 in Granada. Thus, it is foreseeable that less BC particles emissions from these sources were injected to the atmosphere in this period.

4.2 BC concentration classification according to cluster analysis

Changes in meteorological and synoptic conditions could affect the monthly evolution of BC concentration for the study period. To analyze this issue, Figure 4 displays the monthly mean temperature (Fig 4a), wind speed (Fig. 4b), and rainfall (Fig 4c) for Granada from 2005 to 2012. Additionally, this figure also shows a plot (Fig 4d) with the BC concentration versus wind speed range in order to analyze if the monthly evolution of BC concentrations

was caused by changes in wind speed, since it is known that high wind speeds are associated with low aerosol concentrations in the study area (Lyamani et al., 2008). In general, mean wind speeds in the study area were higher in spring and summer seasons and slightly lower in autumn and winter seasons (Fig.4b). Consequently, one may expect higher BC concentrations in winter and autumn than in spring and summer (Figure 2). This assumption is verified in Fig. 4d which shows low BC concentrations for high wind speed classes. The low wind speed classes 0.1-0.3 and 0.3-0.5 m/s were the most representative of Granada local emissions, being less influenced by regional and long range transport.

The influence of changes in air mass patterns on the monthly evolution BC concentrations was also analyzed in detail. Fig. 5a shows the centroids of cluster classification coincident with BC observation days from 2005 to 2012. The air mass types were classified according to the cluster analysis. This plot displays that there were different air mass patterns during the study period. Most of the air mass (34%) corresponds to air mass from local and regional origin (cluster 1). A rather significant fraction (31%) corresponds to air mass from northern direction (cluster 2), while those originated from Mediterranean area (cluster 3) and Atlantic Ocean (cluster 4) were less frequent, 17% and 19%, respectively. Aerosol aging and deposition processes were not included in the back trajectory analysis which could slightly overestimate the role of long-range BC transport. In our study the estimation of BC aging and deposition can become very difficult because BC aerosols came from two different BC sources, anthropogenic BC and biomass burning BC emissions. The aging process of anthropogenic BC may be faster than that of biomass burning BC (Shen et al., 2014).

Monthly evolution of BC concentrations as function of the air mass pattern flows are showed in Fig. 5b. Obviously, BC concentrations were strongly affected by the air mass origin. In the analyzed period, the highest BC concentrations were observed for local air mass (cluster 1) and the lowest concentrations were obtained during Atlantic air mass arrivals (cluster 4). Intermediate BC concentrations were associated with Mediterranean and Northern advections. Local BC sources are mainly dominated by traffic throughout the year, with an additional contribution from residential heating during the winter. Titos et al. (2014), in a study about different aerosol sources affecting to the aerosol concentration levels in Granada, retrieved that anthropogenic aerosol predominantly affected the fine fraction and the traffic is the main source to target in Granada throughout the year, but especially in winter. However, biomass burning aerosol transported from Mediterranean areas may also affect the BC concentration levels mainly in autumn. In this sense, Figure 6 shows the seasonal air mass frequency and BC concentration, respectively, according to the cluster classification. The acceptable correlation between air mass frequency and BC concentration for cluster 1 in winter (Fig. 6a and 6e) and autumn (Fig. 6d and 6h) indicates that just when local air mass affected Granada, BC concentration levels were increased. Air mass frequency included in cluster 2 showed good correlation with BC concentration in winter (Fig. 6a and 6e) and spring (Fig. 6b and 6f). Therefore, part of the total BC load in the atmospheric column in these seasons could be originated from urban-industrial aerosols transported from north Spain and Europe. On the other hand, high BC concentrations were found in autumn just when air mass frequency for cluster 3 was more elevated suggesting that air masses coming from Mediterranean region transport biomass burning particles towards Granada (Fig. 6d and 6h).

In order to complete information about BC concentration for air masses were classified in cluster 1 we show the wind rose diagrams in Figures 7a and 7b. These two plots show the wind rose for the daytime, for the years 2005 to 2012 were separated in two categories, high and low BC concentration levels, respectively. Southeasterly and south-southeasterly winds dominate at high BC concentration values with a 28% and 25% combined occurrence, respectively (Fig. 7a). Wind flowing from these directions crossed over the highway surrounding the city. The wind rose shows that winds from the north-northeasterly directions were the most frequent, when low BC concentration values were found for cluster 1(Fig. 7b). The north-northeasterly wind occurred about 33% of the whole period. Less frequent winds were from the northerly and northwesterly directions, with combined occurrence around 23% and 14%, respectively.

To evaluate the seasonal variability, Fig. 8 analyzes in detail two particular cases according to two flow patterns (cluster 1 and 3). The high BC concentrations observed in winter were likely due to the increase in BC emissions caused by the increase in anthropogenic activities associated with domestic heating and road traffic as well as to unfavorable meteorological conditions like shallow atmospheric boundary layer and low wind speed. Figure 8a shows the surface pressure at mean sea level for 1 January 2012 generated by NOAA Air Resources Laboratory (http://ready.arl.noaa.gov/). This plot is representative of the conditions prevailing from 1 to 5 January when maximum BC concentrations were found. Small pressure gradients took place over the Iberian Peninsula during these days coinciding with a high-pressure system located over Spain. This situation blocks the entry of air masses from the Atlantic and promotes stagnation conditions, reducing the ventilation of the atmosphere. The pressure gradient at the surface over the Iberian Peninsula was very

low and, consequently, there was an absence of wind with cloudless and dry conditions. On the other hand, part of the BC concentration found in Granada mainly in autumn could be related to biomass burning transported from Centre-Europe and Mediterranean region. In this sense, high BC concentrations were found in September in 2008 when air masses were coming from different European-Mediterranean areas transporting biomass burning aerosol from different forest fires in this region. From 22 August to the end of this month 2008 western Iberian Peninsula, south France and north Italy suffered numerous forest fires (see http://maps.geog.umd.edu, and www.fire.uni-freiburg.de). Back trajectory analysis shows that, at least at two altitudes, the study area was affected by European-Mediterranean air masses. According to the NAAPS aerosol transport model the multiple forest fires in different regions in southern Europe, especially in Italy (http://maps.geog.umd.edu) and the associated anticyclonic situation favored rather high levels of smoke over the whole Iberian Peninsula and much of the Mediterranean basin during this period. Thus, the wind flows that arrived at study area at 500 and 1500m could have transported biomass burning particles and/or urban-industrial aerosols originated in south Europe (Fig. 8b).

4.3 Shortwave aerosol radiative forcing

Aerosol optical properties and radiative forcing values were separately derived for composite aerosol and for BC as explained previously. The evolution of the monthly mean values of the daily radiative forcing for composite aerosols (equation 8) from 2005 to 2012 is shown in Figure 9a. This plot shows the monthly forcing values at surface and TOA together with the variation of the atmospheric radiative forcing derived from the difference between the surface and TOA forcing values (e.g, Valenzuela et al., 2012). Composite

aerosol radiative forcing at the surface (ARF_{Surf}) was higher during warm season (up to -28±8 W/m^2 in August), which may be due to larger AOD values recorded during these months. Thus, ARF_{Surf} was well correlated with the observed AODs. The highest monthly mean values of the aerosol radiative forcing at the TOA (ARF_{TOA}) were retrieved in spring and early summer with the highest monthly value in May (4±2 W/m^2). Positive ARF_{TOA} indicates a net warming effect, which mainly arises due to highly reflecting continental surface albedo and strong aerosol absorption. ARF_{TOA} may be affected by other optical parameters such as single scattering albedo, ω (Kedia et al., 2016). The ω values were lower for composite aerosol during spring and summer, indicating enhanced presence of absorbing particles during this period (not shown). Negative values of the ARF_{Surf} indicate a cooling effect, while positive values of the ARF_{TOA} suggest less radiation scattered into space. The difference between ARF_{TOA} and ARF_{Surf} provides the atmospheric radiative forcing for composite aerosol (ARF_{Atm}), which showed the same pattern that ARF_{Surf} with larger mean values in summer (up to 30±3 W/m^2 in July).

The AOD (440 nm) obtained exclusively for BC aerosol showed values ranging between 0.01 and 0.05 (not shown), contributing to about 10-15% of the composite AOD. To determine the impact of BC aerosol on the Earth-atmosphere radiation budget over Granada, radiative forcing for BC aerosols is evaluated (equation 9) and compared to the forcing for composite aerosol. Similarly, figure 9b shows monthly values of forcing at surface ($BCRF_{Surf}$), TOA ($BCRF_{TOA}$) and atmosphere ($BCRF_{Atm}$) estimated exclusively for BC aerosol over the station. In this study the magnitude of the AOD (not shown) and concentration of BC were relatively higher during winter(mean AOD = 0.05±0.02 mean BC = 3.8±0.6 mg/m^2) than for other seasons.

It can be seen that BC radiative forcing exhibits a similar pattern with lower values at surface and higher values at TOA as compared to those for composite aerosol during the entire period. In contrast to composite aerosol, $BCRF_{TOA}$ exhibited similar pattern as BC AOD because BC and $\omega(\lambda)$ values showed no significant changes during all seasons (not shown). Estimated monthly mean $BCRF_{TOA}$ was high in during summer (up to +7.5±0.7 W/m^2 in July). During the whole period, $BCRF_{TOA}$ was positive, which implies a net warming effect due to the absorption of solar radiation by BC aerosol. In addition, $BCRF_{Surf}$ values ranged between -10±1 (January) and -18±3 (July) W/m^2. The negative sign of forcing values observed at the surface implies a net cooling effect. Finally, the positive $BCRF_{Atm}$ values (between +13±1 and +26±3 W/m^2) indicate a net warming effect in the atmosphere. This positive forcing represents a considerable amount of heating of the lower atmosphere and has been conjectured as potential factor causing global warming during winter (Jacobson, 2001).

The mean ARF_{Atm} and $BCRF_{Atm}$ values, averaged over the entire period, were about +23±6 W/m^2 and +15±6 W/m^2, respectively. These forcing values are translated into a heating rate of +0.21±0.06 K/day (composite aerosol) and +0.15±0.06 K/day (BC aerosol). Taking into account only mean values of ARF_{Atm} and $BCRF_{Atm}$, it can be seen that BC radiative forcing in the atmospheric column contributed on average around 67% of total composite aerosol forcing for the study period. This large contribution of BC induced atmospheric warming together with cooling surface. This situation can lead to inversions inhibiting thermal conventions and, in addition to a reduction in the process of cloud formation (Panicker et al., 2013; Chou et al., 2002). There are few studies in the literature reporting contribution of BC to composite aerosol radiative forcing (S. Ramachandran, S. Kedia, 2011; Arola et al.,

2015). For instance, Panicker et al. (2013) found a BC contribution of up to 88% in South Korea. These same authors found lower BC contribution values in an urban India site of up to 55%.

In spite of the fact that our study was constrained to fine mode-dominate cases, ARF_{Surf}, ARF_{TOA} and ARF_{Atm} show values in the range of those found by other authors (Panicker et al., 2010; Ramachandran and Kedia, 2010; Ramachandran et al., 2011). Valenzuela et al. (2012b) focused on desert dust events over Granada station, reporting higher mean values of aerosol radiative forcing at surface (~-19±7 W/m^2), negative mean aerosol radiative forcing values at TOA (~-6±5 W/m^2), and lower mean values in the atmosphere (~14±7 W/m^2), during 2005-2010 period. Therefore, desert dust events contributed to diminish atmospheric warming in Granada station. In contrast to composite aerosol forcing, $BCRF_{Surf,}$ $BCRF_{TOA}$ and $BCRF_{Atm}$ values were higher over Granada than in other regions (Panicker et al., 2010; Panicker et al., 2013). These differences could be justified for the methodological differences in retrieving BC concentration. Large database over closely gridded stations are required in order to quantify the BC aerosol radiative effects over a particular region. Nevertheless, in the present study we attempted to present the scenario of seasonal BC aerosol radiative forcing due to the presence of BC aerosol over an urban typical location on the southeastern Iberian Peninsula.

5. Conclusions

The BC concentration values presented in this study were retrieved for the period 2005-2012. BC concentrations showed high average values in January (4.0±2.6 mg/m^2) and December (4.2±3.3 mg/m^2) and low average values in July (1.6±1.2 mg/m^2) and August

(2.0±0.6 mg/m^2,). The winter average BC concentration (3.8±0.7 mg/m^2) was 30% higher than the eight-year average (2.9±0.9 mg/m^2) whereas the summer average BC concentration (1.9±0.3 mg/m^2) was 35% lower than the overall mean. The reduction in the use of fossil fuels due to economic crisis contributed significantly to reduce BC particles injected to the atmosphere. According to our analysis this situation persisted until 2010. Air masses arriving from four different sectors labeled cluster 1 (local), cluster 2 (north Spain-south Europe), cluster 3 (Mediterranean region) and cluster 4 (Atlantic Ocean) exhibited different BC concentrations. The BC concentration in cluster 1 showed high correlation with air masses frequency of this cluster in winter and autumn. In these seasons BC the traffic source is combined with emissions by domestic heating that were accumulated in the rather shadow boundary layer. High BC concentrations were found in autumn just when air masses frequency for cluster 3 was larger, thus suggesting that air masses coming from Mediterranean region transported biomass burning particles towards Granada. The analysis of a particular case confirm that air masses coming from Europe-Mediterranean region are responsible of the transport of biomass burning particles just when numerous forest fires affected southern France and northern Italy. The lowest BC concentration was associated with the strongest influence of Atlantic Ocean air masses influence, really frequent during spring and summer. The influence of air masses was evident in the BC concentration values and it should be considered when assessing the influence of BC concentrations.

BC optical properties were retrieved from BC fraction together with aerosol AERONET size volume distribution values under the assumption of spherical shape (Mie theory). Aerosol optical properties for composite aerosol (including only fine mode-dominated cases) were derived from AERONET network in agreement with those BC retrievals. BC

and composite aerosol optical properties were used as input in SBDART model in order to obtain radiative forcing values. The mean atmospheric aerosol radiative forcing for composite aerosol, averaged for the entire period, was +23±6 W/m^2 (which translates into a heating rate of +0.21±0.06 K/day) and +15±6 W/m^2 for BC aerosol (which translates into a heating rate of +0.15±0.06 K/day). BC radiative forcing in the atmospheric column contributed on average around 67% of total composite aerosol forcing for the study period taking into account only mean values of ARF_{Atm} and $BCRF_{Atm}$,. This large contribution of BC induced atmospheric warming together with cooling surface.

ACKNOWLEDGMENTS— This work was supported by the Andalusia Regional Government through project P12-RNM-2409, by the Spanish Ministry of Economy and Competitiveness through projects CGL2013-45410-R and CGL2016-81092-R and by the European Union's Horizon 2020 research and innovation programme through project ACTRIS-2 (grant agreement No 654109).The authors thankfully acknowledge the FEDER program for the instrumentation used in this work. Antonio Valenzuela thanks Universidad de Granada for the award of a postdoctoral grant ("Plan Propio. Programa 8. Convocatoria 2014"). The work is co-funded by the European Union through the European Regional Development Fund, included in the COMPETE 2020 (Operational Program Competitiveness and Internationalization) through the ICT project (UID / GEO / 04683/2013) with the reference POCI-01-0145-FEDER-007690. CIMEL Calibration was performed at the AERONET-EUROPE calibration center, supported by ACTRIS (European Union Seventh Framework Program (FP7/2007-2013) under grant agreement no. 262254. The authors express gratitude to the NOAA Air Resources Laboratory (ARL) for the HYSPLIT transport and dispersion model (http://ready.arl.noaa.gov/HYSPLIT.php).

REFERENCES

Ackerman, A. S., Toon, O. B., Stevens, D. E., Heymsfield, A. J., Ramanathan, V., and Welton, E. J., 2000. Reduction of tropical cloudiness by soot, Science, 288(5468), 1042–1047, doi:10.1126/science.288.5468.1042.

Antón, M., Valenzuela, A., Cazorla, A., Gil, J. E., FernándezGálvez, J., Lyamani, H., Foyo-Moreno, I., Olmo, F. J., and Alados-Arboledas, L., 2012. Global and diffuse shortwave irradiance during a strong desert dust episode at Granada (Spain), Atmos. Res., 118, 232–239, doi:10.1016/j.atmosres.2012.07.007.

A. Arola, G.L. Schuster, M.R.A. Pitkänen, O. Dubovik, H. Kokkola, A.V. Lindfors, T. Mielonen, T. Raatikainen, S. Romakkaniemi, S.N. Tripathi, H. Lihavainen, 2015. Direct radiative effect by brown carbon over the Indo-Gangetic Plain Atmos Chem Phys, pp. 12731–12740 http://dx.doi.org/10.5194/acp-15-12731-2015.

Arola, A., Schuster, G., Myhre, G., Kazadzis, S., Dey, S. and Tripathi, S. N., 2011. Inferring absorbing organic carbon content from AERONET data. Atmos. Chem. Phys. 215-225.

Balkanski, Y. J., D. J. Jacob, G. M. Gardner, W. C. Graustein, and K. K. Turekian. 1993. Trans-port and residence times of tropospheric aerosols inferred from a global three-dimensional simulation of 210Pb, J. Geophys. Res., 98, 20,573–20,586.

Babu, S.S., Satheesh, S.K., Krishna Moorthy, K., 2002. Enhanced aerosol radiative forcing due to aerosol black carbon at an urban site in India. Geophys. Res. Let. 29, http://dx.doi.org./10.1029/2002GL015826.

Bond, T. C., D. G. Streets, K. F. Yarber, S. M. Nelson, J.-H. Woo, and Z. Klimont, 2004. A technology-based global inventory of black and organic carbon emissions from combustion, J. Geophys. Res., 109, D14203, doi:10.1029/2003JD003697.

Bond, T.C., Doherty, S.J., Fahey, D.W., Forster, P.M., Berntsen, T., DeAngelo, B. J., Flanner, M.G., Ghan, S., Kärcher, B., Koch, D., Kinne, S., Kondo, Y., Quinn, P.K., Sarofim, M.C., Schultz, M.G., Schulz, M., Venkataraman, C., Zhang, H., Zhang, S., Bellouin, N., Guttikunda, S. K., Hopke, P. K., Jacobson, M.Z., Kaiser, J.W., Klimont, Z., Lohmann, U., Schwarz, J.P., Shindell, D., Storelvmo, T., Warren, S.G. and Zender, C.S., 2013. Bounding the role of black carbon in the climate system: A scientific assessment. J. Geophys. Res. doi:10.1002/jgrd.50171.

Bohren, C.F., Huffman, D.R., 1998. Absorption and Scattering of Light by Small Particle. Wiley, New York.

Bush, B.C., and Valero, F.P.J., 2003. Surface aerosol radiative forcing at Gosan during the ACE-Asia campaign, J. Geophys. Res. 108, D23, 8660, doi: 10.1029/2002JD003233.

Cao, J., Zhu, C., Chow, J.C.,Watson, J.G., Han, Y.,Wang, G., Shen, Z., An, Z., 2009. Black carbon relationships with emissions and meteorology in Xi'an, China. Atmos. Res. 94, 194-202.

Chou, M. D., Chan, P. K. and Wang, M., 2002. Aerosol radiative forcing derived from sea WiFS retrieved aerosol optical properties. J. Atmos. Sci. 59, 748-757.

Chung, S. H., and J. H. Seinfeld, 2005. Climate response of direct radiative forcing of anthropogenic black carbon, J. Geophys. Res., 110, D11102, doi:10.1029/2004JD005441.

Cachorro, V.E., C. Toledano, N. Prats, M. Sorribas, S. Mogo, A. Berjón, B. Torres, R. Rodrigo, J. de la Rosa, and A. M. De Frutos, 2008. The strongest desert dust intrusion mixed with smoke over the Iberian Peninsula registered with Sun photometry, J. Geophys. Res. 113, D14S04, doi:10.1029/2007JD009582.

Dey, S., Tripathi, S. N., Singh, R. P. and Holben, B., 2006. Retrieval of black carbon and specific absorption over Kanpur city, Northern India during 2001-2003 using AERONET data. Atmos. Environ. 40(3), 445-456.

Derimian, Y., Karnieli, A., Kaufman, Y.J., Andreae, M.O., Andreae, T.W., Dubovik, O., Maenhaut, W., Koren, I., 2008. The role of iron and black carbon in aerosol light absorption. Atmos.Chem.Phys. 8, 3623-3637.

Dubovik, O., Smirnov, A., Holben, B.N., King, M.D., Kaufman, Y.J., Eck, T.F., I. Slutsker, I., 2000. Accuracy assessment of aerosol optical properties retrieved from Aerosol Robotic Network (AERONET) Sun and sky radiance measurements, J. Geophys. Res. 105, D8, 9791-9806.

Dubovik, O., Sinyuk, A., Lapyonok, T., Holben, B.N., Mishchenko, M., Yang, P., Eck, T.F., Volten, H., Muñoz, O., Veihelmann, B., van der Zande, W.J., Leon, J.F., Sorokin, M., Slutsker, I., 2006. Application of spheroid models to account for aerosol particle nonsphericity in remote sensing of desert dust. J. Geophys. Res. 111, D11208, doi:10.1029/2005JD006619, 2006.

Dubovik, O., and King M. D., 2000. A flexible inversion algorithm for retrieval of aerosol optical properties from sun and sky radiance measurements, J. Geophys. Res. 105, 20,673–20,696.

Draxler, R.R., Hess, G.D., 1998. An overview of the HYSPLIT_4 modelling system for trajectories, dispersion and deposition. Aust. Meteorological Mag. 47, 295-308.

Draxler, R. R., B. Stunder, G. Rolph, and A. Taylor (2009), HYSPLIT_4 User's Guide, NOAA Air Resour. Lab., Silver Spring, Md.

Eck, T. F., Holben, B. N., Reid, J. S., Dubovik, O., Smirnov, A., O'Neill, N. T., Slutsker, I., and Kinne, S., 1999. Wavelength dependence of optical depth of biomass burning, urban, and desert dust aerosols, J. Geophys. Res. 104, 31 333–31 349.

Estellés, V., Martinez-Lozano, J.A., Utrillas, M.A.P., 2007. Influence of air mass history on the columnar aerosol properties at Valencia, Spain. J. Geophys. Res. 112, D15211, doi:10.1029/2007JD008593.

Granados-Muñoz, M. J., Navas-Guzman, F., Bravo-Aranda, J. A., Guerrero-Rascado, J. L., Lyamani, H. and co-authors. 2012. Automatic determination of the planetary boundary layer height using lidar: one-year analysis over southeastern Spain. J. Geophys. Res. Atmos. 117, D18208, 1-10.

Hansen, J., Sato, M., Ruedy, R., Lacis, A., and Oinas, V., 2000. Global warming in the twenty-first century: an alternative scenario, P. Natl. Acad. Sci. USA, 97, 9875–9880.

Harris, J., Draxler, R. R. and Oltmans, S. J., 2005. Trajectory model sensitivity to differences in input data and vertical transport method, J. Geophys. Res. 110, D14109, doi:10.1029/2004JD005750.

Haywood, J.M. and Shine, K.P. 1997. The effect of anthropogenic sulfate and soot aerosol on the clear sky planetary radiation budget. Geophys. Res. Lett. 22, 603-6.

Holben, B.N., Eck, T.F., Slutsker, I., Tanre, D., Buis, J.P., Setzer, A., Vermote, E., Reagan, J.A., Kaufman, Y.J., Nakajima, T., Lavenu, F., Jankowiak, I., Smirnov, A., 1998. AERONET - A federated instrument network and data archive for aerosol characterization. Remote Sens. Environ. 66, 1-16.

Jacobson, M. Z. 2001. Strong radiative heating due to mixing state of black carbon on atmospheric aerosols, Nature, 409, 695– 697.

Jacobson, M. Z., 2006. Effects of absorption by soot inclusions within clouds and precipitation on global climate, J. Phys. Chem., 110, 6860–6873.

Jacobson, M. Z., 2012. Investigating cloud absorption effects: Global absorption properties of black carbon, tar balls, and soil dust in clouds and aerosols, J. Geophys. Res., 117, D06205, doi:10.1029/2011JD017218.

Johnson, B. T., K. P. Shine, and P. M. Forster, 2004. The semidirect aerosol effect: Impact of absorbing aerosols on marine stratocumulus, Q. J. Roy. Meteor. Soc., 130(599), 1407–1422, doi:10.1256/qj.03.61.

Jones, A., J.M. Haywood, and O. Boucher, 2007. Aerosol forcing, climate response and climate sensitivity in the Hadley Centre climate model, J. Geophys. Res., 112, D20211, doi:10.1029/2007JD008688.

Kanakidou, M., Seinfeld, J. H., Pandis, S. N., Barnes, I., Dentener, F. J., Facchini, M. C., Van Dingenen, R., Ervens, B., Nenes, A., Nielsen, C. J., Swietlicki, E., Putaud, J. P., Balkanski, Y., Fuzzi, S., Horth, J., Moortgat, G. K., Winterhalter, R., Myhre, C. E. L., Tsigaridis, K., Vignati, E., Stephanou, E. G., and Wilson, J., 2005. Organic aerosol and global climate modelling: a review, Atmos. Chem. Phys., 5, 1053-1123, doi:10.5194/acp-5-1053-2005.

Kedia S., Cherian R., Islam S., Das S.K. & Kaginalkar A., 2016. Regional simulation of aerosol radiative effects and their influence on rainfall over India using WRFChem model. Atmos. Res., 182, 232-242.

Keil, A., Wendisch, M., Brüggemann, E., 2001. Measured profiles of aerosol particle absorption and its influence on clear-sky solar radiative forcing. J. Geophys. Res. 106, 1237-1247.

Kirchstetter, T. W., Novakov, T., Hobbs, P. V., 2004. Evidence that the spectral dependence of light absorption by aerosols is affected by organic carbon. J. Geophys. Res. 109, D21208, http://dx.doi.org/10.1029/2004JD004999.

Kirchstetter, T.W., Aguiar, J., Tonse, S., Fairley, D., Novakov, T., 2008. Black carbon densities and diesel vehicle emission factors derived from coefficient of haze measurements in California: 1967e2003. Atmos. Environ. 42, 480-491.

Kokkalis P., Amiridis V., Allan J.D., Papayannis A., Solomos S., Binietoglou I., Bougiatioti A., Tsekeri A., Nenes A., Rosenberg P.D., Marenco F., Marinou E., Vasilescu J., Nicolae D., Coe H., Bacak A. & Chaikovsky A., 2017. Validation of LIRIC aerosol concentration retrievals using airborne measurements during a biomass burning episode over Athens. Atmos. Res. 183, 255-267.

Koch, D. and Del Genio, A. D., 2010. Black carbon semi-direct effects on cloud cover: review and synthesis, Atmos. Chem. Phys., 10, 7685–7696, doi:10.5194/acp-10-7685-2010.

Kumar Bharath, d. and S. Verma, 2016. Potential emission flux to aerosol pollutants over Bengal Gangetic plain through combined trajectory clustering and aerosol source fields analysis, Atmos. Res. 178–179, http://dx.doi.org/10.1016/j.atmosres.2016.04.012.

Kumar M., Raju M.P., Singh R.K., Singh A.K., Singh R.S. & Banerjee T., 2017. Wintertime characteristics of aerosols over middle Indo-Gangetic Plain: Vertical profile, transport and radiative forcing. Atmos. Res. 183, 268-282.

Liu, J. F., Fan, S. M., Horowitz, L. W., and Levy, H., 2011. Evaluation of factors controlling long-range transport of black carbón to the Arctic, J. Geophys. Res.-Atmos., 116, D04307, doi:10.1029/2010jd015145.

Lyamani, H., Olmo, F.J., Alados-Arboledas, L., 2008. Light scattering and absorption properties of aerosol particles in the urban environment of Granada, Spain. Atmos. Environ. 42, 2630-2642.

Lyamani, H., Olmo, F.J., Alados-Arboledas, L., 2010. Physical and optical properties of aerosols over an urban location in Spain: seasonal and diurnal variability. Atmos. Chem. Phys. 10, 239-254.

Lyamani, H., Olmo, F.J., Foyo, I. and Alados-Arboledas, L., 2011. Black carbón aerosols overa n urban área in south-eastern Spain: Changes detected after the 2008 economic crisis. Atmos. Environ. 6423-6432.

Lyamani, H., Fernandez-Galvez, J., Perez-Ramirez, D., Valenzuela, A., Anton, M., Alados, I., Titos, G., Olmo, F.J., Alados-Arboledas, L., 2012. Aerosol properties over two urban sites in South Spain during an extended stagnation episode in winter season. Atmos. Environ. 62, 424-432. doi: 10.1016/j.atmosenv.2012.08.050.

Liou, K.N.: An introduction to Atmospheric Radiation. Elsevier, New York, 583 pp.

Olmo, F.J., Quirantes, A., Alcantara, A., Lyamani, H., Alados-Arboledas, L., 2006. Preliminary results of a non-spherical aerosol method for the retrieval of the atmospheric aerosol optical properties. J. Quant. Spectrosc. Radiat. Transfer. 100, 305-314.

Oshima, N., Koike, M., Zhang, Y., Kondo, Y., Moteki, N., Takegawa, N., and Miyazaki, Y., 2009. Aging of black carbon in outflow from anthropogenic sources using a mixing state resolved model: Model development and evaluation, J. Geophys. Res., 114, D06210, doi:10.1029/2008JD010680.

Panicker, A. S., G. Pandithurai, et al., 2010. On the contribution of black carbon to the composite aerosol radiative forcing over an urban environment. Atmos. Environ. 44(25), 3066-3070.

Panicker, A. S., S.-H. Park, et al., 2013. Observations of Black Carbon characteristics and radiative forcing over a Global Atmosphere Watch supersite in Korea. Atmos. Environ. 77, 98-104.

Pereira, S.N., F. Wagner, and A.M. Silva, 2011. Seven years of measurements of aerosol scattering properties, near the surface, in the southwestern Iberia Peninsula, Atmos. Chem. Phys. 11, 17-29.

Prats, N., Cachorro, V.E., Sorribas, M., Mogo, S., Berjon, A., Toledano, C., De Frutos, A.M., de la Rosa, J., Laulainen, N., de la Morena, B.A., 2008. Columnar aerosol optical properties during "El Arenosillo 2004 summer campaign". Atmos. Environ. 42, 2643-2653.

S. Ramachandran, S. Kedia, 2011. Aerosol radiative effects over an urban location and a remote site in western India: seasonal variability. Atmos. Environ., 45, pp. 7415–7422.

Ramachandran, S., Rajesh, T.A., 2007. Black carbon aerosol mass densities over Ahmedabad, an urban location in western India: comparison with urban sites in Asia, Europe, Canada, and the United States. J. Geophys. Res. 112, D06211. doi:10.1029/2006JD007488.

Ramanathan, V. and Carmichael, G. 2008. Global and regional climate changes due to black carbon. Nature Geos. 1, 221-227. http://dx.doi.org/10.1038/ngeo156.

Ricchiazzi, P., S. Yang, C. Gautier, and D. Sowle., SBDART: A research and teaching software tool for plane-parallel radiative transfer in the Earth's atmosphere, Bull. Am. Meteorol. Soc., 79, 2101– 2114, 1998.

Saha, A., Despiau, S., 2009. Seasonal and diurnal variations of black carbon aerosols over a Mediterranean coastal zone. Atmos. Res. 92, 27e41.

Schuster, G. L., Dubovik, O., Holben, B.N. and Clothiaux, E. E., 2005. Inferring black carbon content and specific absorption from Aerosol Robotic Network (AERONET) aerosol retrievals, J. Geophys. Res. 110, D10S17, doi:10. 1029/2004JD004548.

Shen, Z., Liu, J., Horowitz, L. W., Henze, D. K., Fan, S., H., L. I., Mauzerall, D. L., Lin, J.-T., and Tao, S., 2014. Analysis of transpacific transport of black carbon during HIPPO-3: implications for black carbon aging, Atmos. Chem. Phys., 14, 6315-6327, doi:10.5194/acp-14-6315-2014.

Silva, A.M ,Von Hoyningen-Huene, W., Bugalho, L., Schmidt,T., Costa, M.J., Heintzenberg, J. 2002. Aerosol Optical Properties from columnar data during ACE2 at the South Coast of Portugal. J. Geophys. Res. Vol.107, Nº D22 4642.

Stohl, A., 1998. Computation, accuracy and applications of trajectories: A review and bibliography, Atmos. Environ. 32, 947–966.

G. Titos, H. Lyamani, M. Pandolfi, A. Alastuey, L. Alados-Arboledas, 2014. Identification of fine (PM_1) and coarse ($PM_{10\ -1}$) sources of particulate matter in an urban environment, Atmos. Environ., 89, pp. 593–602.

Toledano, C., Cachorro, V.E., de Frutos, A.M., Torres, B., Berjon, A., Sorribas, M., Stone, R.S., 2009. Airmass Classification and Analysis of Aerosol Types at El Arenosillo (Spain). J. Appl. Meteorol. Climatol. 48, 962-981.

Valenzuela, A., Olmo, F.J., Lyamani, H., Antón, M., Quirantes, A., Alados-Arboledas, L., 2012a. Classification of aerosol radiative properties during African desert dust intrusions over southeastern Spain by sector origins and cluster analysis, J. Geophys. Res. 117, D06214, doi:10.1029/2011JD016885.

Valenzuela, A., Olmo, F.J., Lyamani, H., Antón, M., Quirantes, A. and Alados-Arboledas, L., 2012b. Aerosol radiative forcing during African desert dust intrusions (2005-2010) over Southeaster Spain. Atmos. Chem. Phys. 12, 10331–10351.

Verma, S., Pani, S.K. and Bhanja, S.N., 2013. Sources and radiative effects of wintertime black carbon aerosols in an urban atmosphere in east India. Chemosphere, 90, 260-269.

Zhang, X. Y., Wang, Y. Q., Niu, T., Zhang, X. C., Gong, S. L., Zhang, Y. M., and Sun, J. Y., 2012. Atmospheric aerosol compositions in China: spatial/temporal variability, chemical signature, regional haze distribution and comparisons with global aerosols, Atmos. Chem. Phys., 12, 779–799, doi:10.5194/acp-12-779-2012.

Zdun A., Rozwadowska A. & Kratzer S., 2016. The impact of air mass advection on aerosol optical properties over Gotland (Baltic Sea). Atmos. Res. 182, 142-155.

Zhao S., Tie X., Cao J. & Zhang Q., 2015. Impacts of mountains on black carbon aerosol under different synoptic meteorology conditions in the Guanzhong region, China. Atmos. Res. 164-165, 286-296.

FIGURES

Figure 1: a) Location of Granada city and, b) radiometric station (CEAMA).

Figure 2: Monthly statistics of BC concentration over Granada from 2005 to 2012 represented as box diagrams. In these box diagrams, the mean is represented by a blank dot

and the median by a middle line. The top/bottom box limits represent the percentiles 25% and 75%. In addition, the error bars of the box are the percentiles 5% and 95%. Number of observations is indicated between parentheses.

Figure 3: Evolution of monthly mean values of (a) Temperature (°C) (b) wind speed (m/s) (c) rainfall (mm) and (d) BC concentrations as function of wind speeds at Granada from December 2005 to November 2008. The error bars are standard deviations.

Figure 4: Annual statistics of BC concentration over Granada from 2005 to 2012 represented as box diagrams. In these box diagrams, the mean is represented by a blank dot and the median by a middle line. The top/bottom box limits represent the percentiles 25% and 75%. In addition, the error bars of the box are the percentiles 5% and 95%.

Figure 5: (a) Centroids of cluster classification at 500 m level coincident with BC observation days, and (b) BC concentrations as function of cluster classification from 2005 to 2012. The error bars are standard deviations.

Figure 6: a-d) Seasonally frequencies of air mass types according with cluster analysis that affected Granada from 2005 to 2012, e-h) seasonally BC concentration values according with cluster analysis that affected Granada from 2005 to 2012.

Figure 7: Wind rose plots for cluster 1 affecting to Granada place with (a) high BC concentration levels, (b) low BC concentration levels.

Figure 8: a) Synoptic chart of surface pressure at mean sea level for 1 January 2012, b) back trajectories ending at Granada at 12 UTC for altitude 500, 1500 and 3000m a.g.l. for 30 August 2008 representing days 22–30.

Figure 9: Radiative forcing at surface, TOA and in the atmosphere for a) Composite aerosol and b) BC aerosol.

FIGURE 1

a)

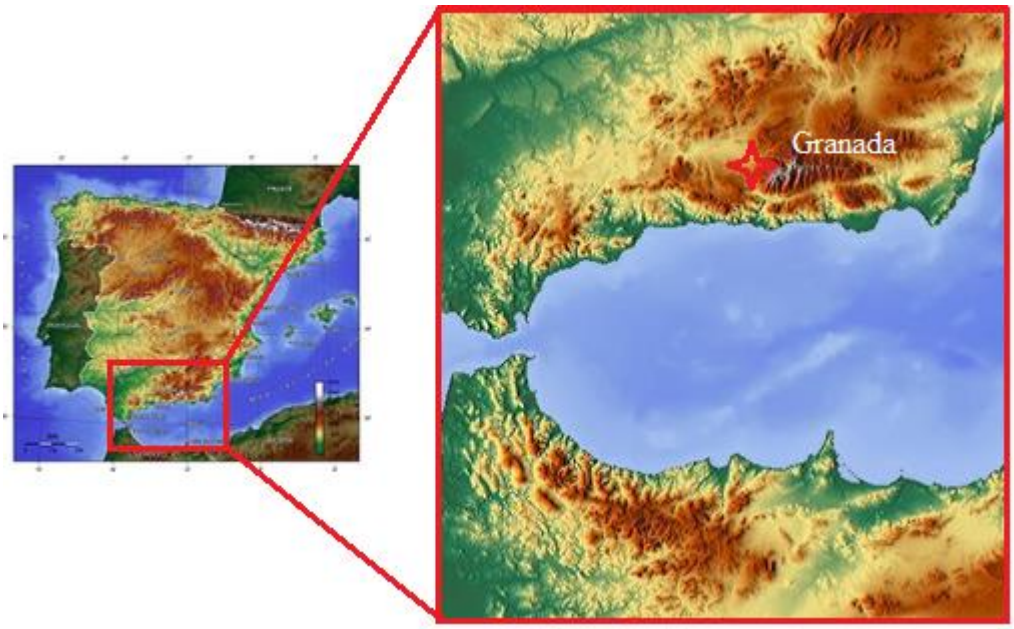

b)

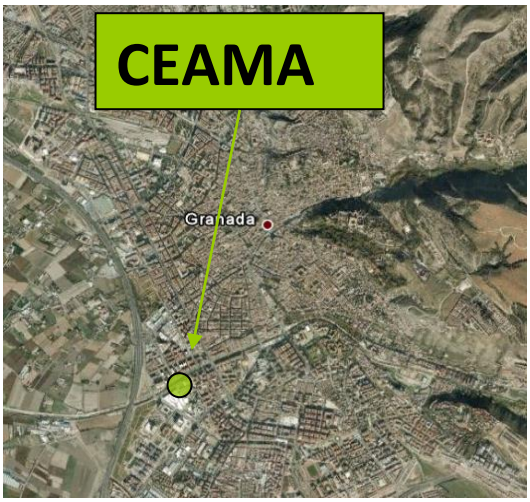

FIGURE 2

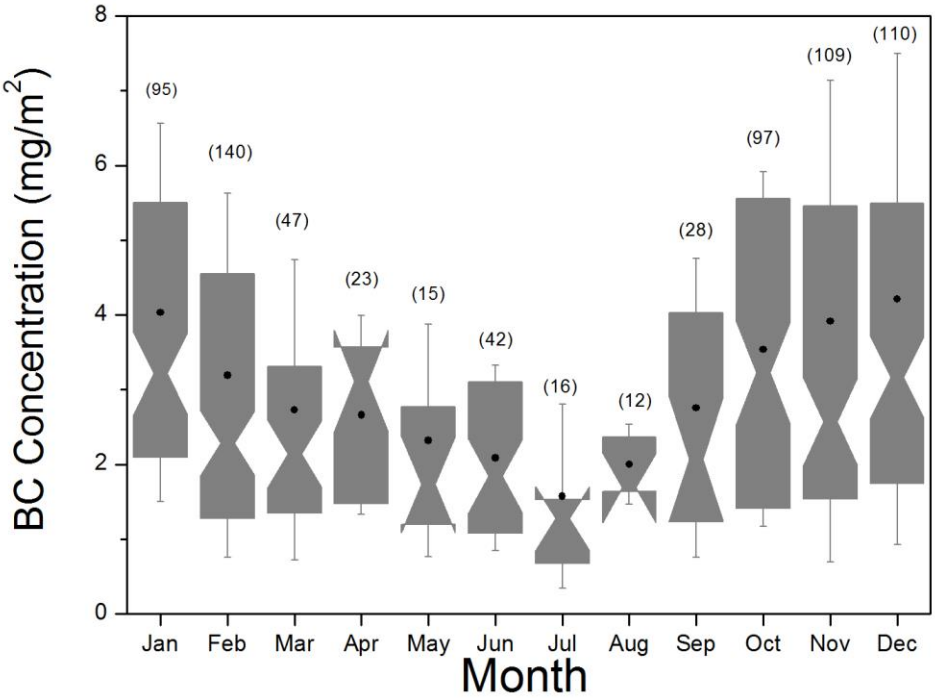
BC Concentration (mg/m2)
8
6
4
2
0
(95)
(140)
(47)
(23)
(15)
(42)
(16)
(12)
(28)
(97)
(109)
(110)
Jan
Feb
Mar
Apr
May
Jun
Jul
Aug
Sep
Oct
Nov
Dec
Month

FIGURE 3

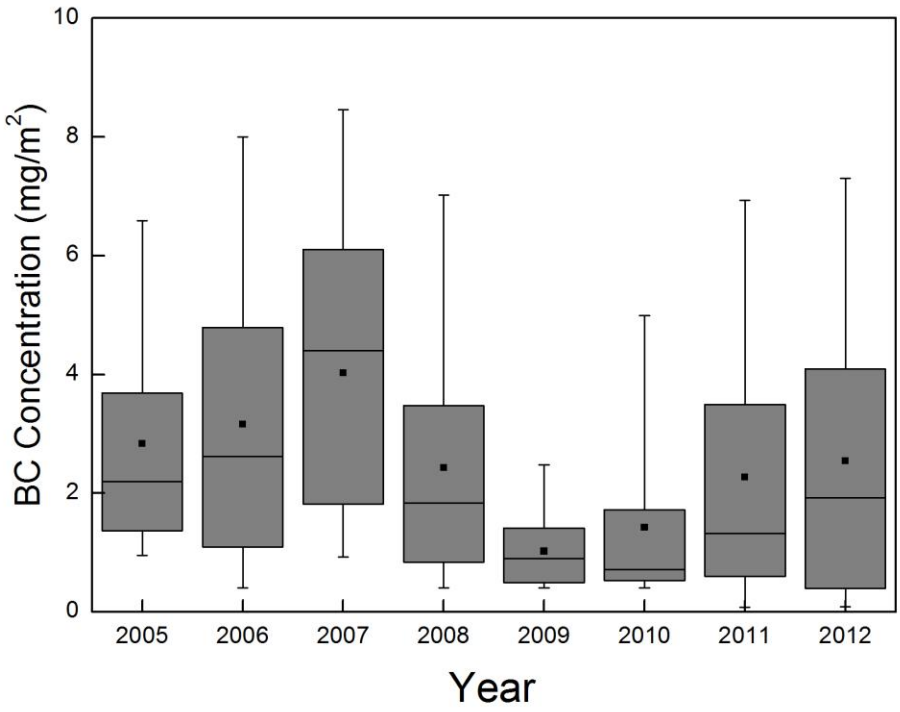
BC Concentration (mg/m2)
0
2
4
6
8
10
2005
2006
2007
2008
2009
2010
2011
2012
Year

FIGURE 4

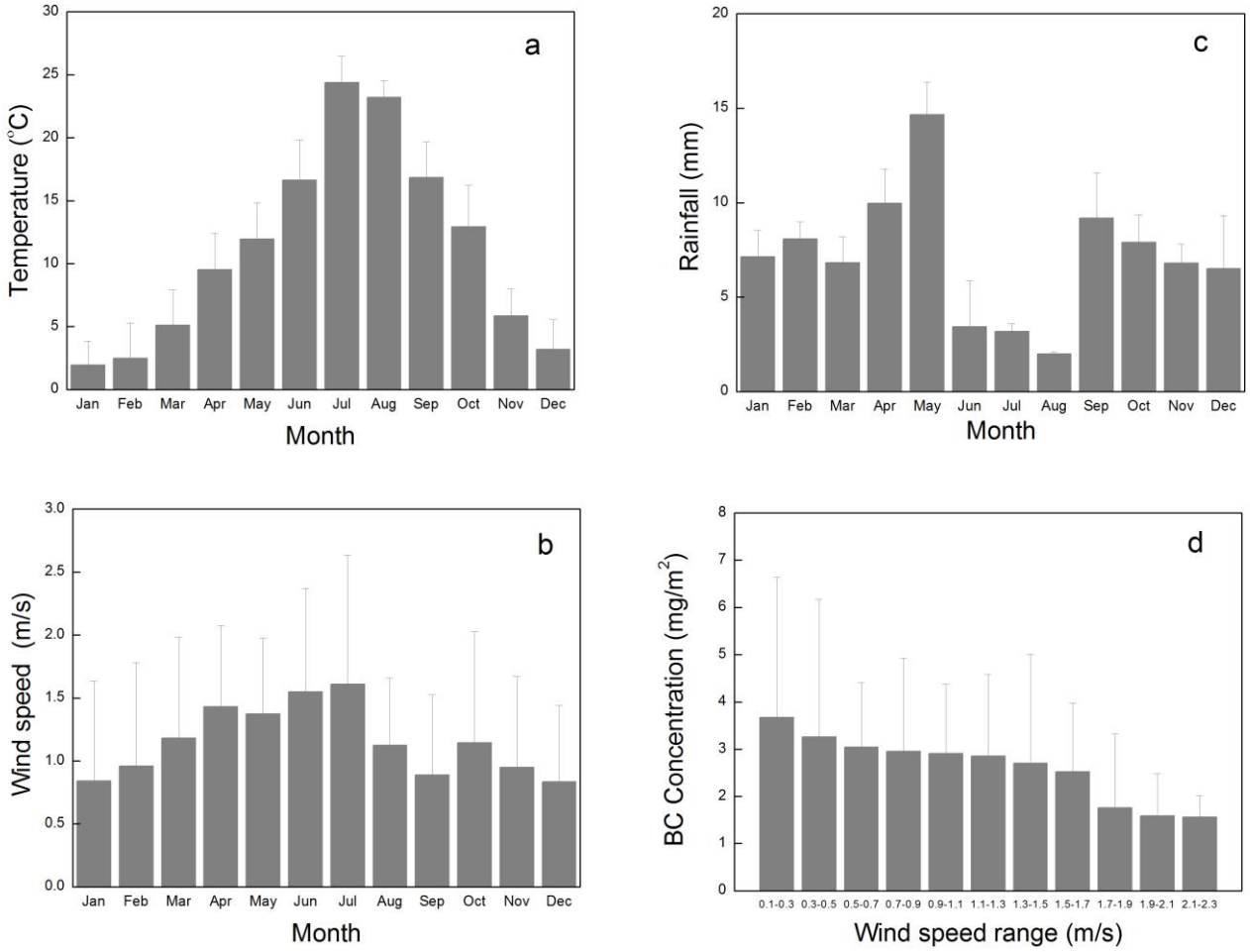
a
Temperature (°C)
Month
Jan Feb Mar Apr May Jun Jul Aug Sep Oct Nov Dec
c
Rainfall (mm)
Month
b
Wind speed (m/s)
Month
d
BC Concentration (mg/m2)
Wind speed range (m/s)
0.1-0.3 0.3-0.5 0.5-0.7 0.7-0.9 0.9-1.1 1.1-1.3 1.3-1.5 1.5-1.7 1.7-1.9 1.9-2.1 2.1-2.3

FIGURE 5

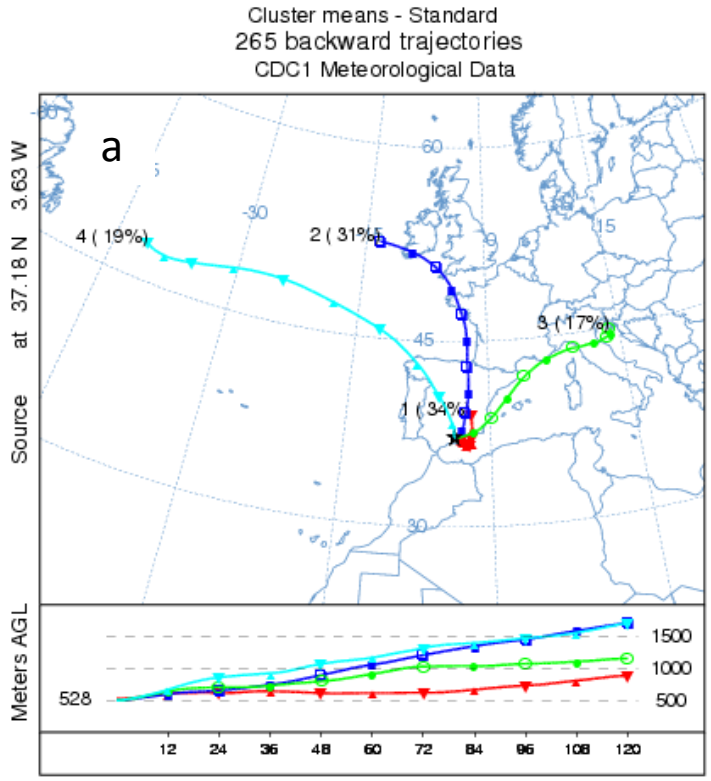
Cluster means - Standard
265 backward trajectories
CDC1 Meteorological Data
a
Source at 37.18 N 3.63 W
4 (19%)
2 (31%)
3 (17%)
1 (34%)
Meters AGL
528
1500
1000
500
12
24
36
48
60
72
84
96
108
120

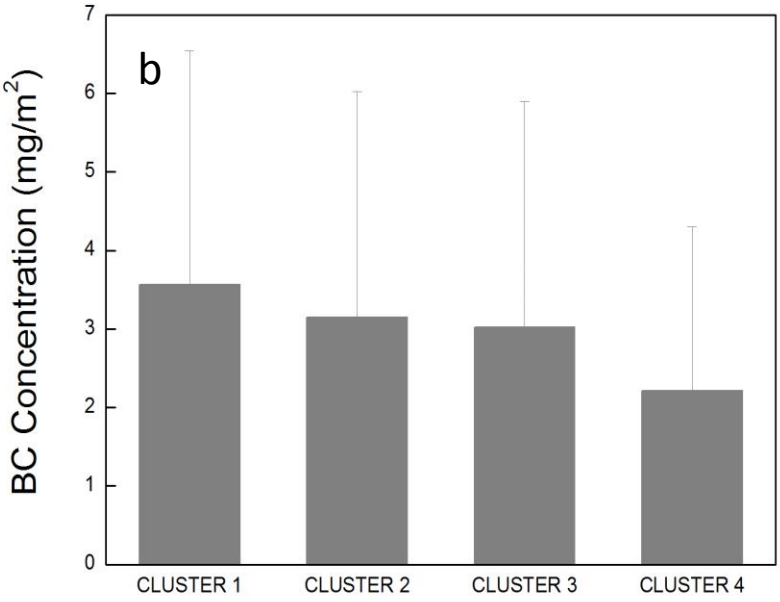
b
BC Concentration (mg/m2)
0
1
2
3
4
5
6
7
CLUSTER 1
CLUSTER 2
CLUSTER 3
CLUSTER 4

FIGURE 6

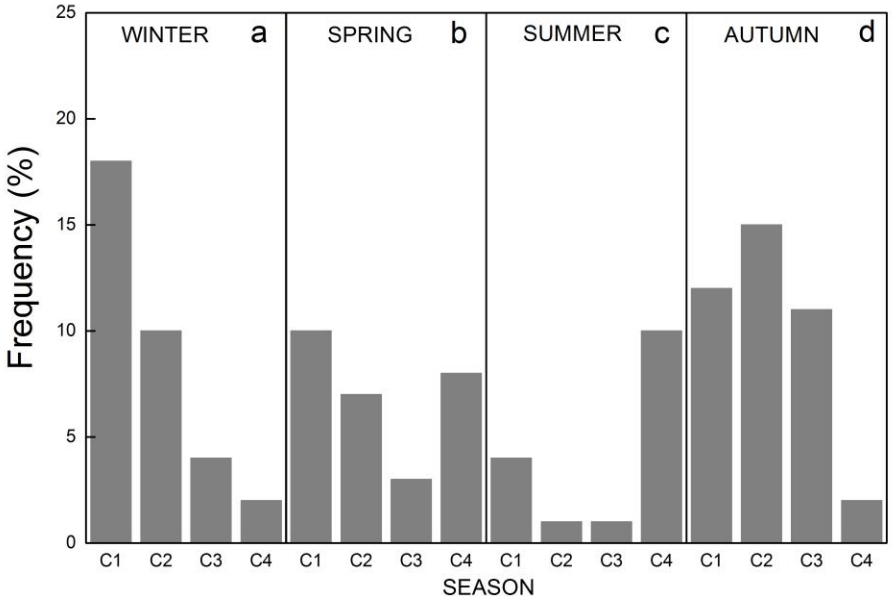
WINTER a
SPRING b
SUMMER c
AUTUMN d
Frequency (%)
0
5
10
15
20
25
C1 C2 C3 C4 C1 C2 C3 C4 C1 C2 C3 C4 C1 C2 C3 C4
SEASON

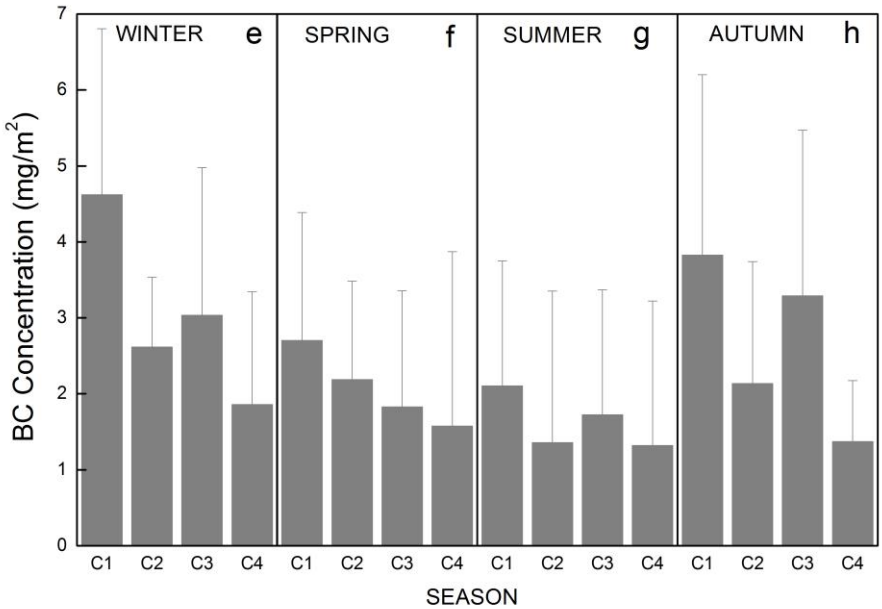
WINTER e
SPRING f
SUMMER g
AUTUMN h
BC Concentration (mg/m2)
0
1
2
3
4
5
6
7
C1 C2 C3 C4 C1 C2 C3 C4 C1 C2 C3 C4 C1 C2 C3 C4
SEASON

FIGURE 7

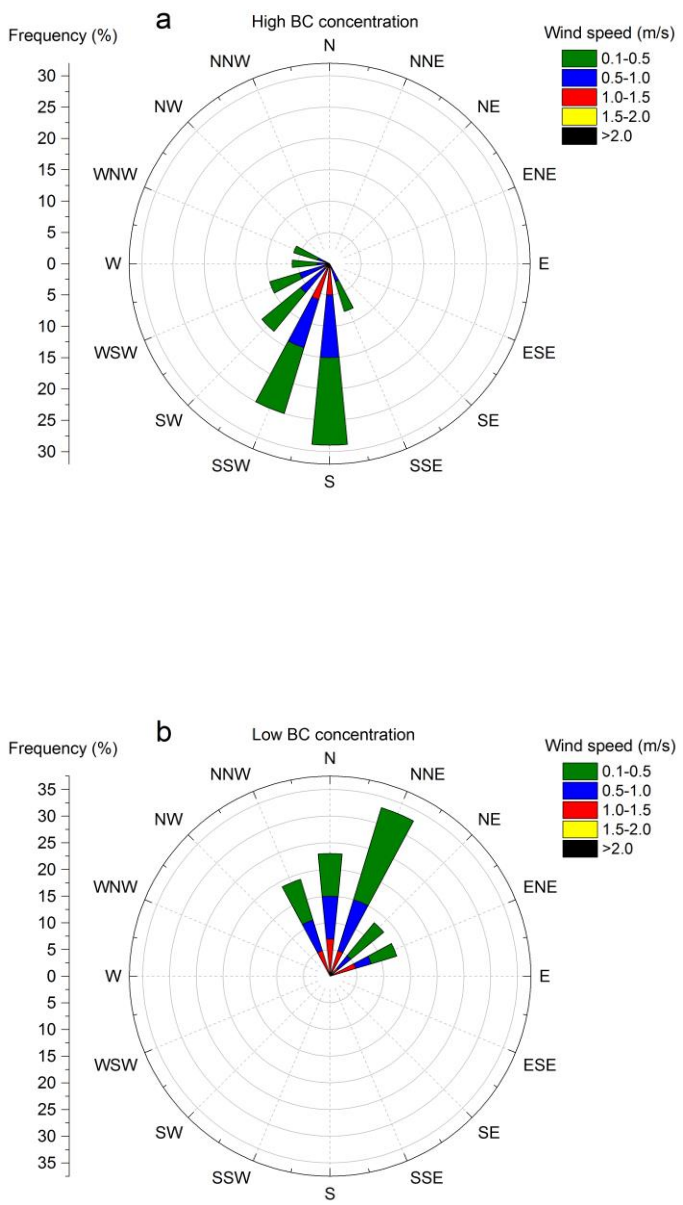
a
High BC concentration
Frequency (%)
Wind speed (m/s)
0.1-0.5
0.5-1.0
1.0-1.5
1.5-2.0
>2.0
N
NNE
NE
ENE
E
ESE
SE
SSE
S
SSW
SW
WSW
W
WNW
NW
NNW
b
Low BC concentration
Frequency (%)
Wind speed (m/s)
0.1-0.5
0.5-1.0
1.0-1.5
1.5-2.0
>2.0

FIGURA 8

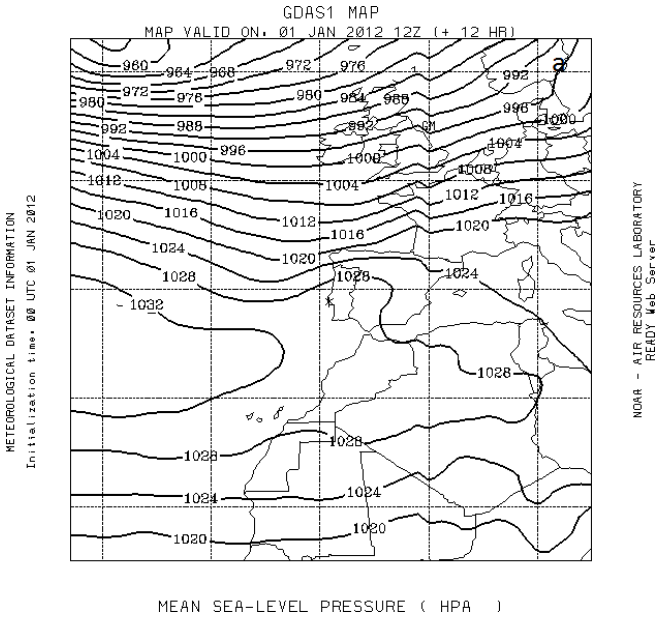
GDAS1 MAP
MAP VALID ON. 01 JAN 2012 12Z (+ 12 HR)
a
METEOROLOGICAL DATASET INFORMATION
Initialization time. 00 UTC 01 JAN 2012
NOAA - AIR RESOURCES LABORATORY
READY Web Server
MEAN SEA-LEVEL PRESSURE (HPA)

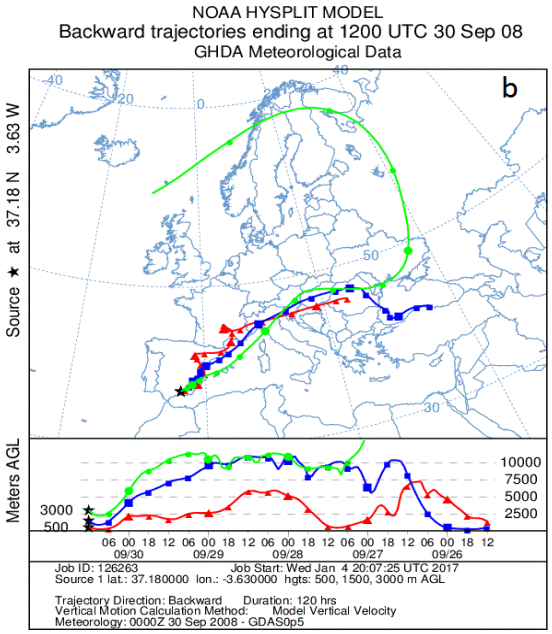
NOAA HYSPLIT MODEL
Backward trajectories ending at 1200 UTC 30 Sep 08
GHDA Meteorological Data
b
Source ★ at 37.18 N 3.63 W
Meters AGL
10000
7500
5000
2500
3000
500
06 00 18 12 06 00 18 12 06 00 18 12 06 00 18 12 06 00 18 12
09/30 09/29 09/28 09/27 09/26
Job ID: 126263 Job Start: Wed Jan 4 20:07:25 UTC 2017
Source 1 lat.: 37.180000 lon.: -3.630000 hgts: 500, 1500, 3000 m AGL
Trajectory Direction: Backward Duration: 120 hrs
Vertical Motion Calculation Method: Model Vertical Velocity
Meteorology: 0000Z 30 Sep 2008 - GDAS0p5

FIGURA 9

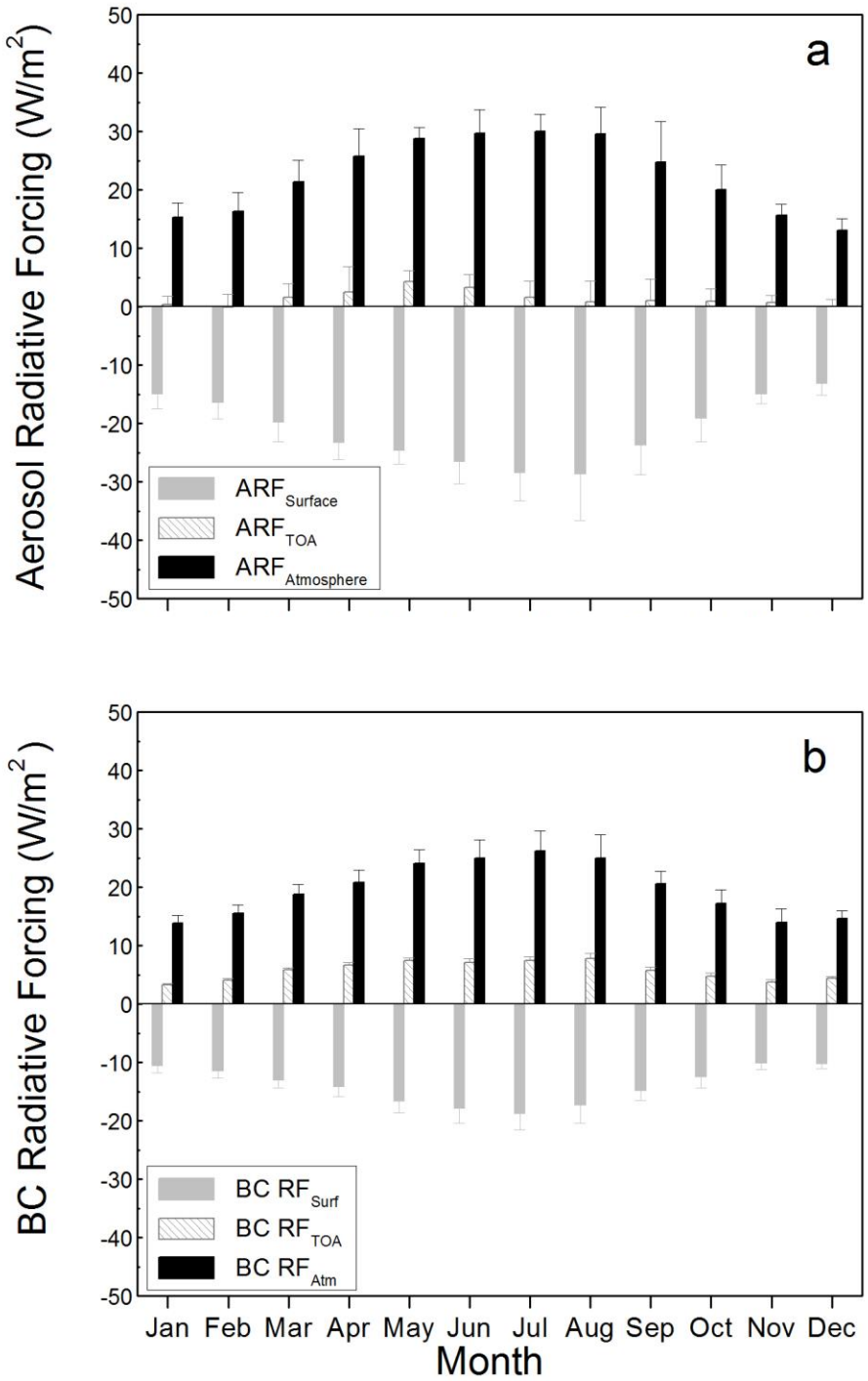
a
Aerosol Radiative Forcing (W/m^2)
ARF$_{Surface}$
ARF$_{TOA}$
ARF$_{Atmosphere}$
b
BC Radiative Forcing (W/m^2)
BC RF$_{Surf}$
BC RF$_{TOA}$
BC RF$_{Atm}$
Jan Feb Mar Apr May Jun Jul Aug Sep Oct Nov Dec
Month